Second-virial theory for shape-persistent living polymers templated by disks

M. Torres Lázaro,[1] R. Aliabadi [2] and H. H. Wensink [1,*]

[1]*Laboratoire de Physique des Solides, UMR 8502, CNRS, Université Paris-Saclay, 91405 Orsay, France*
[2]*Physics Department, Sirjan University of Technology, Sirjan 78137, Iran*

Living polymers composed of noncovalently bonded building blocks with weak backbone flexibility may self-assemble into thermoresponsive lyotropic liquid crystals. We demonstrate that the reversible polymer assembly and phase behavior can be controlled by the addition of (nonadsorbing) rigid colloidal disks which act as an entropic reorienting "template" onto the supramolecular polymers. Using a particle-based second-virial theory that correlates the various entropies associated with the polymers and disks, we demonstrate that small fractions of discotic additives promote the formation of a polymer nematic phase. At larger disk concentrations, however, the phase is disrupted by collective disk alignment in favor of a discotic nematic fluid in which the polymers are dispersed antinematically. We show that the antinematic arrangement of the polymers generates a nonexponential molecular-weight distribution and stimulates the formation of oligomeric species. At sufficient concentrations the disks facilitate a liquid-liquid phase separation which can be brought into simultaneously coexistence with the two fractionated nematic phases, providing evidence for a four-fluid coexistence in reversible shape-dissimilar hard-core mixtures without cohesive interparticle forces. We stipulate the conditions under which such a phenomenon could be found in experiment.

I. INTRODUCTION

Supramolecular "living" polymers are composed of aggregating building blocks that are joined together via noncovalent bonds. The polymers can break and recombine reversibly as the typical attraction energy between monomers is comparable to the thermal energy [1,2]. Elementary (Boltzmann) statistical mechanics then tells us that the polymers must be in equilibrium with their molecular weight distribution which emerges from a balance between the association energy and mixing entropy of the polymers. This results in a wide range of different polymeric species with an exponential size distribution whose shape is governed primarily by temperature and monomer concentration. Reversible polymers are thus distinctly different from usual "quenched" polymers whose molecular weight distribution is fixed by the conditions present during the synthesis process.

Reversible association is ubiquitous in soft matter. Examples include the formation of various types of micellar structures from block copolymers [3,4], hierarchical self-assembly of short-fragment DNA [5,6], chromonic mesophases [7,8] composed of noncovalently stacked sheet-like macromolecules, and the assembly of amyloid fibrils from individual proteins [9]. Microtubules, actin and other biofilaments provide essential mechanical functions in the cell and consist of dynamically organizing molecular units that self-organize into highly interconnected structures [10].

A particularly interesting case arises when the monomers associate into shape-persistent, directed polymers [11]. In-terpolymer correlations then become strongly orientation-dependent and may drive the formation of liquid crystals. Spontaneous formation of lyotropic liquid crystals has been observed, for example, in long wormlike micelles under shear [12], oligomeric DNA [13], and chromonics [7]. When the monomer concentration exceeds a critical value, the polymers grow into strongly elongated aggregates and an (isotropic) fluid of randomly oriented polymers may spontaneously align into, for instance, a nematic liquid crystal characterized by long-range orientational correlations without structural periodicity [14]. While aggregation-driven nematization has been contemplated also for thermotropic systems [15], our current focus is on lyotropic systems composed of rigid polymers suspended in a fluid host medium, where the isotropic-nematic phase transition can be rationalized on purely entropic grounds in terms of a gain of volume-exclusion entropy upon alignment at the expense of orientational entropy [16–18]. However, this argument becomes more convoluted in the case of directed, reversible polymers where the trade-off between these two entropic contributions is connected to a simultaneous maximization of the mixing entropy and the number of monomer-monomer linkages. In particular, the coupling between orientational order and polymer growth turns out to be a very important one; collective alignment leads to longer polymers, which tend to align even more strongly thus stimulating even further growth [19]. Recent simulation studies have basically corroborated this scenario [20–22].

An intriguing question in relation to the above is the following: Can the hierarchical organization of reversible polymers be controlled by the addition of nonadsorbing shape-dissimilar components that affect the way they align? Indeed, for chromonics it is known that the presence of

---

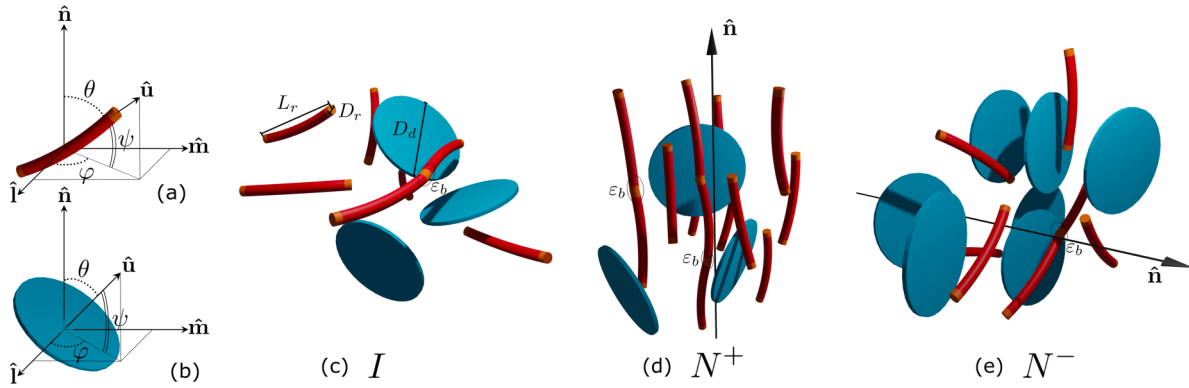*Corresponding author: rik.wensink@universite-paris-saclay.fr

FIG. 1. Schematic representation of the various liquid crystal phases emerging for disks mixed with polymerizing rods. (a), (b) Principal angles describing the orientation $\hat{\mathbf{u}}$ of a single rod monomer and disk with respect to the molecular director $\hat{\mathbf{n}}$ with θ denoting the polar angle, φ the azimuthal angle, and $\psi = \frac{\pi}{2} - \theta$ the meridional angle. (c) Isotropic phase; (d) polymer uniaxial nematic phase N^+; (e) discotic uniaxial nematic phase N^- in which the reversibly polymerizing rods are dispersed antinematically.

additives can bring about condensation or reorientation of the reversible stacks, thereby changing their phase behavior through subtle modifications of the system entropy [23]. Recent experiments on clay nanosheets mixed with reversibly polymerizing tubuline rods have demonstrated that these mixtures remain stable against flocculation and provide a test bed for exploring entropy-driven phase behavior of biopolymer-platelet mixtures [24]. Furthermore, it is well established that mixing prolate (rod-shaped) colloids with their oblate counterparts generates a strong coupling between the orientations of both components leading to organizations with mixed nematic and antinematic symmetries. Numerous theoretical studies starting with the early work of Alben [25] have attempted to rationalize the intricate isotropic-nematic phase behavior of these mixtures placing particular emphasis on stabilizing the highly sought-after biaxial nematic phase in which both components are aligned along mutually perpendicular directions thus generating a fluid with an orthorhombic (D_{2h}) symmetry [26–36]. Similar kinds of antinematic or biaxial symmetries could arise when dispersing rod-shaped colloids in a thermotropic liquid crystal under appropriate anchoring conditions [37,38]. Antinematic order has been shown to naturally emerge in porous smectic structures of shape-persistent nanorings [39,40] or may be realized with the help of external electromagnetic fields as was demonstrated for clay nanosheets [41] and for disks in the presence of associating magnetic beads [42]. In this study we wish to build upon the preceding concepts and explore hierarchical self-organization of reversible polymers in the presence of disk-shaped particles. An example of colloidal disks that could be envisaged are clay nanosheets that consist of nanometer-thick discotic particles with a very high diameter-to-thickness ratio. These particles find widespread use in industrial soft matter and are at the basis of many colloidal-polymer composite materials [43,44]. The clay sheets on their own, provided they do no gelate in crowded conditions, have a natural tendency to align and form various types of liquid crystals, including nematic phases [45–48]. When mixed with reversibly polymerizing components in the absence of strong disk-polymer attractions, the disks not only induce orientational "templating" of the supramolecular polymers [49], they also influence the mixing

entropy of the system which must have consequences for polymer growth and phase behavior [50,51]. It is precisely these combined entropic effects that we wish to examine more closely in this work. To this end, we formulate a simple model (Sec. II) that we subsequently cast into a particle-based theory (Sec. III) that features reversible association and accounts for all relevant entropic contributions on the approximate second-virial level. The orientation degrees of freedom of the species are treated using a number of simplified variational approaches that render our theory algebraically manageable. We stress that our primary attention in this work goes to mixed-shape nematic phases and we do not consider partially crystallized states that may become stable at elevated packing conditions where our theoretical approach is no longer applicable.

Our study broadly falls into two parts. In the first part (Sec. IV) we explore the molecular weight distribution in mixtures in which the polymers are organized either nematically or *antinematically*. The latter state can be realized at elevated disk concentrations where correlations between the disks are strong enough to generate nematic order of the discotic subsystem which in turn, enforces the supramolecular rods to align perpendicular to the discotic director in such a way that the overall system retains its uniaxial $D_{\infty h}$ point group symmetry [Fig. 1(e)]. Whereas reversible polymers in a conventional nematic organization are distributed along a near-exponential form with minor nonexponential corrections at short lengths [21], we argue that *antinematic* living polymers may, under certain conditions, exhibit a strong nonexponential weight distribution with the most-probable polymer size being oligomeric rather than monomeric.

In the second part of the paper (Secs. V and VI) we explore the isotropic-nematic phase behavior of the mixed systems by focusing on the uniaxial nematic phases, which seems to be the prevailing nematic symmetry for strongly shape-dissimilar mixtures [27,31,33,35,52]. Our theoretical model is generic and should be applicable to a wide range of different monomer-disk size ratios and temperatures. We discuss the key features for a few exemplary mixtures. One of them is a distinct azeotrope that develops for the isotropic-polymer nematic coexistence, suggesting a strong

orientational templating effect imparted by volume-excluded interactions between the polymers and the disks. Furthermore, under certain disk-monomer size constraints, a remarkable four-phase equilibria appears involving a simultaneous coexistence of isotropic gas and liquid phases along with two fractionated uniaxial nematic phases. In Sec. VII we discuss our findings in relation to recent colloid-polymer models where similar multiphase equilibria have been reported. We end this work with formulating the main conclusions along with some perspectives for further research in Sec. VIII.

II. MODEL

In this study, we focus on mixtures of tip-associating rod-shaped monomers with limited backbone flexibility mixed with rigid disks. An overview of the basic particle shapes is given in Fig. 1. We assume that each rod monomer is equipped with identical attractive patches at either tip such that each rod end can only form a single bond with an adjacent rod tip producing a linear polymer. The rods do not associate into multiarmed or ring-shaped polymers. We further assume that all species retain their basic fluid order such that the respective density distributions remain uniform in positional space (but not necessarily in orientational phase space). We do not account for the possibility of hexagonal columnar phases formed by (pure) polymers at high monomer concentration and low temperature combined with elevated polymer backbone flexibility [50,53]. In fact, disks too may form columnar structures at packing fraction exceeding typically 40% [54–56], which goes beyond the concentration range we consider relevant here. Interactions between the polymer segments and the disks are assumed to be purely hard with the only energy scale featuring in the model being the noncovalent bond energy ε_b between the monomers.

Contrary to previous modeling studies of rod-disks mixture we focus here solely on uniaxial nematic phases and ignore the possibility of biaxial order in which both components align along mutually perpendicular directors. Our focus is motivated by the expectation that excluded-volume interactions between the polymers and the disks, which are the principal entropic forces behind generating nematic order [16], are too disparate to guarantee such orthorhombic nematic symmetry to be stable. Previous theoretical studies [32,33,35,36,52] as well as experiments [57–59] and simulations [27,34,60] on mixed-shape colloids suggest that strongly unequal excluded volumes indeed favor demixing into strongly fractionated uniaxial nematic phases. In view of the basic symmetry difference between the linear polymer and disk, we then anticipate a rod-based uniaxial phase [denoted N^+; Fig. 1(d)] in which the disks are distributed antinematically throughout the uniaxial matrix. Conversely, when the disks outnumber the polymers, a disk-based uniaxial nematic [N^-; Fig. 1(e)] is formed in which the aggregating rods adopt antinematic order.

III. SECOND-VIRIAL THEORY FOR REVERSIBLE POLYMERS MIXED WITH RIGID DISKS

We start with formulating the free energy per unit volume V of a mixture of disks with density $\rho_d(\hat{\mathbf{u}})$ and reversibly polymerizing rods. We define $\rho_r(\ell, \hat{\mathbf{u}})$ as the number density

of monomer segments aggregated into a polymeric rod with contour length ℓL and orientation described by unit vector $\hat{\mathbf{u}}$. The aggregation number or polymerization degree is specified by the index $\ell = 1, 2, 3, \ldots$. Let us write the free energy per unit volume of the mixture as follows [21,61]:

$$\frac{F}{V} \sim \sum_\ell \int d\hat{\mathbf{u}} \{\ln[4\pi \Lambda_r \rho_r(\ell, \hat{\mathbf{u}}) \ell^{-1}] - 1\} \ell^{-1} \rho_r(\ell, \hat{\mathbf{u}})$$
$$+ \int d\hat{\mathbf{u}} \{\ln[4\pi \Lambda_d \rho_d(\hat{\mathbf{u}})] - 1\} \rho_d(\hat{\mathbf{u}}) + \frac{F_{as}}{V} + \frac{F_{wlc}}{V} + \frac{F_{ex}}{V}.$$
$$(1)$$

Without loss of generality, all energies are implicitly expressed in units of thermal energy $k_B T$ (with k_B Boltzmann's constant and T temperature). Furthermore, $\Lambda_{r/d}$ are the thermal volumes of the species which are immaterial for the thermodynamic properties we are about to explore. The factor 4π is included for convenience and equals the unit sphere surface representing the orientational phase space. The total rod monomer concentration ρ_{r0} is a conserved quantity so that $\rho_{r0} = \sum_\ell \int d\hat{\mathbf{u}} \rho_r(\ell, \hat{\mathbf{u}})$. Likewise, $\rho_{d0} = \int d\hat{\mathbf{u}} \rho_d(\hat{\mathbf{u}})$ represents the number density of disks. The first two terms are related to the ideal gas or mixing entropy and describe the ideal translation and orientational entropy of each polymer and disk, respectively. The third contribution in Eq. (1) represents an association energy that drives end-to-end aggregation of the monomer segments. It reads:

$$\frac{F_{as}}{V} = \varepsilon_b \sum_\ell \int d\hat{\mathbf{u}} \ell^{-1} \rho_r(\ell, \hat{\mathbf{u}})(\ell - 1). \quad (2)$$

The free energy per unit volume arising from the polymerized rod segments follows from the bond potential ε_b between two adjacent rod segments and the number density $\rho_a(\ell, \hat{\mathbf{u}}) = (1/\ell)\rho_r(\ell, \hat{\mathbf{u}})$ of polymers with aggregation number ℓ each containing $\ell - 1$ bonds. Being normalized to the thermal energy the potential ε_b serves as an *effective* temperature scale. At strongly reduced temperature ($\varepsilon_b \ll 0$) the association energy is minimised when all monomers join together into a single long polymer, while at high temperature ($\varepsilon_b \gg 0$) polymerization is strongly suppressed. If $-\varepsilon_b$ is of the order of the thermal energy $k_B T$, the single chain configuration is highly unfavorable in view of the mixing entropy that favors a broad distribution of aggregates with strongly disperse contour lengths. This we will explore more systematically in Sec. IV.

A. Backbone flexibility

The second last term in Eq. (1) represents the effect of polymer flexibility through a correction to the original orientational entropy [first term in Eq. (1)] that accounts for the internal configurations of a so-called wormlike chain [18]. This leads to a strongly nonlinear term with respect to the segment density [21,62]:

$$\frac{F_{wlc}}{V} = -\frac{2L_r}{3\ell_p} \sum_\ell \int d\hat{\mathbf{u}} [\rho_r(\ell, \hat{\mathbf{u}})]^{1/2} \nabla^2 [\rho_r(\ell, \hat{\mathbf{u}})]^{1/2}, \quad (3)$$

where ∇^2 denotes the Laplace operator on the unit sphere. The persistence length ℓ_p measures the typical length scale

over which local orientational fluctuations of the segments are correlated. In our model we assume that the rod segments are only slightly flexible [62] so that $\ell_p \gg \ell$ suggesting that the main orientational entropy stems from the rigid body contribution that is subsumed into the ideal gas term in Eq. (1). The wormlike chain correction vanishes in the somewhat unnatural situation where all polymers, irrespective of their contour length, are perfectly rigid and the persistence length tends to infinity ($\ell_p \to \infty$).

B. Excluded-volume entropy

The last contribution in Eq. (1) is the excess free energy that incorporates all excluded-volume driven interactions between the stiff polymers and disks. Assuming all interactions to be strictly hard, we write following Ref. [26]:

$$\frac{F_{ex}}{V} = \frac{1}{2} \sum_{\ell,\ell'} \iint d\hat{\mathbf{u}} \, d\hat{\mathbf{u}}' \rho_r(\ell, \hat{\mathbf{u}}) \rho_r(\ell', \hat{\mathbf{u}}') 2L_r^2 D_r |\sin\gamma|$$
$$+ \sum_{\ell} \iint d\hat{\mathbf{u}} \, d\hat{\mathbf{u}}' \rho_r(\ell, \hat{\mathbf{u}}) \rho_d(\hat{\mathbf{u}}') \frac{\pi}{4} L_r D_d^2 |\cos\gamma|$$
$$+ \frac{1}{2} \iint d\hat{\mathbf{u}} \, d\hat{\mathbf{u}}' \rho_d(\hat{\mathbf{u}}) \rho_d(\hat{\mathbf{u}}') \frac{\pi}{2} D_d^3 |\sin\gamma|, \qquad (4)$$

where $L_{r,d}$ and $D_{r,d}$ denote the length and diameter of the cylindrical building blocks [see Fig. 1(b)]. We assume all polymers and disks to be sufficiently slender, i.e., $L_r/D_r \gg 1$ and $D_d/L_d \gg 1$ so that finite-thickness corrections to the excluded volume terms above can be neglected. Next we formally minimize the free energy with respect to the polymer segment distribution:

$$\frac{\delta}{\delta \rho_r(\ell, \hat{\mathbf{u}})} \left(\frac{F}{V} - \lambda_r \sum_{\ell} \int d\hat{\mathbf{u}} \rho_r(\ell, \hat{\mathbf{u}}) \right) = 0 \qquad (5)$$

and to the one-body density of the disks:

$$\frac{\delta}{\delta \rho_d(\hat{\mathbf{u}})} \left(\frac{F}{V} - \lambda_d \int d\hat{\mathbf{u}} \rho_d(\hat{\mathbf{u}}) \right) = 0. \qquad (6)$$

The Lagrange multipliers $\lambda_{r,d}$ ensure that the total concentration of each species (monomers and disks) be preserved. The coupled Euler-Lagrange (EL) equations can be rendered tractable by expanding the orientation-dependent kernels that depend on the enclosed angle γ between the main particle orientation axes, as we will show next.

IV. MOLECULAR WEIGHT-DISTRIBUTION FROM SECOND-POLYNOMIAL APPROXIMATION

A commonly employed method to cast the free energy in a more tractable form is to express the trigonometric functions featuring in the excluded-volume (4) in terms of a bilinear expansion in Legendre polynomials [63–65]. Truncating this expansion after the second-order contribution leads to a simplified theory that has been explored previously for rod-plate mixtures [26,52] as well as in the context of rods with fixed length polydispersity [66]. For the present mixture, the approximation should be adequate if the nematic order of either

component is not too strong. We write:

$$|\sin\gamma| = \frac{\pi}{4} - \frac{5\pi}{32} \mathcal{P}_2(\cos\theta) \mathcal{P}_2(\cos\theta') + \cdots$$
$$|\cos\gamma| = \frac{1}{2} + \frac{5}{8} \mathcal{P}_2(\cos\theta) \mathcal{P}_2(\cos\theta') + \cdots$$

in terms of the second Legendre polynomials $\mathcal{P}_2(x) = \frac{3}{2}x^2 - \frac{1}{2}$. The orientation of each particle is described by a polar angle θ and azimuthal angle φ defined with respect to the nematic director $\hat{\mathbf{n}}$ [see Figs. 1(a) and 1(b)]. Let us define a set of *size-specific* nematic order parameters for the polymer:

$$S_{r\ell} = \rho_{r\ell}^{-1} \int d\hat{\mathbf{u}} \rho_r(\ell, \hat{\mathbf{u}}) \mathcal{P}_2(\hat{\mathbf{u}} \cdot \hat{\mathbf{n}}) \qquad (7)$$

with $\rho_{r\ell} = \int d\hat{\mathbf{u}} \rho_r(\ell, \hat{\mathbf{u}})$ a partial number density of rod segments belonging to polymers of length ℓL. Likewise we find for the disks:

$$S_d = \rho_{d0}^{-1} \int d\hat{\mathbf{u}} \rho_d(\hat{\mathbf{u}}) \mathcal{P}_2(\hat{\mathbf{u}} \cdot \hat{\mathbf{n}}). \qquad (8)$$

These order parameters allow us to distinguish between an isotropic fluid ($S_{r\ell} = S_d = 0$), a polymer-dominated uniaxial nematic fluid (N^+: $S_{r\ell} > 0$, $S_d < 0$) and a discotic one (N^-: $S_r < 0$, $S_d > 0$), as sketched in Figs. 1(d) and 1(e), respectively. With the aid of these expansions, the excess free energy can be written in terms of a simple bilinear dependence on the nematic order parameter:

$$\frac{F_{ex}}{V} \sim \rho_{r0}^2 \left(1 - \frac{5}{8} \bar{S}_r^2 \right) + 2q\rho_{r0}\rho_d \left(1 + \frac{5}{4} \bar{S}_r S_d \right)$$
$$+ z\rho_d^2 \left(1 - \frac{5}{8} S_d^2 \right). \qquad (9)$$

Here we have implicitly renormalized the free energy and species densities in terms of the isotropic excluded volume of the monomeric rods $v_{rr} = \frac{\pi}{4} L_r^2 D_r$. The excess free energy thus depends only on the excluded-volume *ratios* $q = v_{rd}/v_{rr}$ and $z = v_{dd}/v_{rr}$ with $v_{rd} = \frac{\pi}{16} L_r D_d^2$ and $v_{dd} = \frac{\pi^2}{16} D_d^3$ denoting the isotropized monomer-disk and disk-disk excluded volumes, respectively. Furthermore, the bar denotes a molecular-weight average of the nematic order parameter associated with the polymers:

$$\bar{S}_r = \rho_{r0}^{-1} \sum_{\ell} \rho_{r\ell} S_{r\ell}. \qquad (10)$$

Similarly, the coupled EL equations may be cast as follows:

$$\ell^{-1} \ln[4\pi \rho_r(\ell, \hat{\mathbf{u}}) \ell^{-1}] = \lambda_r + \varepsilon_b \ell^{-1} + a_r \mathcal{P}_2(\hat{\mathbf{u}} \cdot \hat{\mathbf{n}})$$
$$+ \frac{L_r}{3\ell_p} \frac{\nabla^2 [\rho_r(\ell, \hat{\mathbf{u}})]^{1/2}}{[\rho_r(\ell, \hat{\mathbf{u}})]^{1/2}} \qquad (11)$$

and

$$\ln[4\pi \rho_d(\hat{\mathbf{u}})] = \lambda_d + a_d \mathcal{P}_2(\hat{\mathbf{u}} \cdot \hat{\mathbf{n}}). \qquad (12)$$

The uniaxial order parameters that feature in the EL equations are specified as follows:

$$a_r = \frac{5}{4}(\rho_{r0}\bar{S}_r - 2q\rho_{d0}S_d),$$
$$a_d = \frac{5}{4}(z\rho_{d0}S_d - 2q\rho_{r0}\bar{S}_r). \qquad (13)$$

We are now equipped to explore the equilibrium polymer length distribution $\rho_{r\ell} = \int d\hat{\mathbf{u}} \rho_r(\ell, \hat{\mathbf{u}})$ corresponding to the basic fluid symmetries we consider (cf. Fig. 1).

A. Isotropic fluid

In the isotropic phase, all nematic order parameters are strictly zero. Applying conservation of monomers to Eq. (11) and performing some algebraic rearrangements we find a geometric distribution (i.e., the discrete analog of the exponential distribution):

$$\rho_{r\ell} = \ell e^{\varepsilon_b + \lambda_r \ell}$$
$$= \ell e^{\varepsilon_b} \left(1 - m_I^{-1}\right)^\ell \qquad (14)$$

in terms of the mean aggregation number:

$$m_I = \frac{\sum_\ell \rho_a(\ell)\ell}{\sum_\ell \rho_a(\ell)} = \frac{1}{2}(1 + \sqrt{1 + 4\rho_{r0} e^{-\varepsilon_b}}), \qquad (15)$$

which, as expected, goes up monotonically with increasing monomer concentration ρ_{r0} and also increases when the effective temperatures ε_b grows more negative. Since there is no global particle alignment whatsoever, the presence of the disks does not influence the polymerization process, and the polymer molecular-weight distribution is independent from the disk concentration.

B. Uniaxial nematic fluid

The decoupling of polymeric rods and disks is no longer valid for a nematic fluid where the alignment direction of one component is strongly affected by the amount of orientational "templating" it experiences from the other component. The polymer density follows from Eq. (11) and can be written in an exponential form:

$$4\pi \rho_r(\ell, \hat{\mathbf{u}}) = \ell \exp[\varepsilon_b + \ell \lambda_r + \tilde{a}_r \ell \mathcal{P}_2(t)] \qquad (16)$$

with $t = \cos\theta$. The three basic contributions affecting the polymer molecular weight distribution in a (uniaxial) nematic fluid are easily identified in the argument; the first denotes monomer-monomer bonding while the second term enforces monomeric mass conservation. The third one is the most interesting one; it encapsulates the templating effect associated with nematization of the disks as per Eq. (13). Here we have introduced a_r as a renormalized version of the one in Eq. (13):

$$\tilde{a}_r = a_r + \xi. \qquad (17)$$

The factor ξ depends on both a_r itself and on the polymer persistence length ℓ_p. It accounts for the finite polymer flexibility and vanishes for strictly rigid polymers ($\ell_p \to \infty$). The corresponding expressions are given in the Appendix. As noted previously, the multiplier λ_r featuring in Eq. (16) follows from monomer mass conservation:

$$\sum_{\ell=1}^{\infty} \int d\hat{\mathbf{u}} \rho_r(\ell, \hat{\mathbf{u}}) = \rho_{r0}. \qquad (18)$$

The summation can be resolved analytically, and we find:

$$\rho_{r0} = e^{\varepsilon_b} \frac{1}{2} \int_{-1}^{1} dt \frac{e^{W(t)}}{(e^{W(t)} - 1)^2}. \qquad (19)$$

The molecular-weight averaged nematic order parameter Eq. (10) is then given by:

$$\bar{S}_r = \rho_{r0}^{-1} e^{\varepsilon_b} \frac{1}{2} \int_{-1}^{1} dt \frac{\mathcal{P}_2(t) e^{W(t)}}{(e^{W(t)} - 1)^2}. \qquad (20)$$

The two conditions above are intricately coupled given that $\tilde{a}_r$ depends on both $\bar{S}_r$ and S_d via Eq. (13). Convergence of the summation in Eq. (18) requires that the argument be negative:

$$W(t) = \lambda_r + \tilde{a}_r \mathcal{P}_2(t) < 0, \quad \text{all } t. \qquad (21)$$

Noticing that $-1/2 \leqslant ||\mathcal{P}_2|| \leqslant 1$ one then finds that λ_r should satisfy:

$$-\lambda_r < |\tilde{a}_r| \quad (N^+),$$
$$-\lambda_r < |\tilde{a}_r/2| \quad (N^-), \qquad (22)$$

and it is tempting to introduce a rescaled normalization constant λ_r' that is strictly positive ($\lambda_r' > 0$) for both phases. With this, we recast:

$$W(t) = \begin{cases} \frac{3}{2}\tilde{a}_r(t^2 - 1) - \lambda_r' & (N^+) \\ \frac{3}{2}\tilde{a}_r t^2 - \lambda_r' & (N^-) \end{cases}. \qquad (23)$$

Unlike for the isotropic phase, the normalization constant λ_r' cannot be resolved in closed form. The molecular-weight distribution of the polymer follows from integrating Eq. (16) over all orientations $\hat{\mathbf{u}}$:

$$\rho_{r\ell} = \ell e^{\varepsilon_b} \frac{1}{2} \int_{-1}^{1} dt\, e^{\ell W(t)}. \qquad (24)$$

The uniaxial nematic order parameter $S_{r\ell}$ associated with a polymer of length ℓ is easily found from:

$$S_{r\ell} = -\frac{1}{2} \left\{ 1 + \frac{1}{\tilde{a}_r \ell} - \frac{1}{F(\sqrt{3\tilde{a}_r \ell/2})\sqrt{\tilde{a}_r \ell/3}} \right\} \qquad (25)$$

in terms of Dawson's integral $F(x) = e^{-x^2} \int_0^x e^{y^2} dy$ [67]. The discotic nematic order parameter S_d easily follows from the above expression upon substituting $\tilde{a}_r \ell \to a_d$. A little reflection of Eq. (25) tells us the following; since a_r does not depend explicitly on the aggregation number ℓ, the nematic order parameter $S_{r\ell}$ must be a monotonically increasing function of the polymerization degree ℓ; the longer the polymers the stronger their nematic ($a_r > 0$) or antinematic ($a_r < 0$) alignment in the mixed nematic fluid. This effect becomes systematically weaker for increasingly flexible polymers as can easily be inferred from the above expression by comparing $S_{r\ell}$ versus ℓ for rigid polymers ($\xi = 0$) versus the case of slightly flexible ones (ξ nonzero but small) for any given value for a_r.

Let us now examine a concrete example by picking a dense uniaxial discotic nematic doped with polymerizing rods. The polymers are dispersed antinematically within the discotic fluid as indicated in Fig. 1(e). In specifying the shape of the rods and disks, we can distinguish between so-called *symmetric* mixtures [26], in which the excluded-volume between two monomers, a monomer and a disk, and two disks are all equal, so that $q = 1$ and $z = 1$ and *asymmetric mixtures* composed of species with strongly disparate excluded-
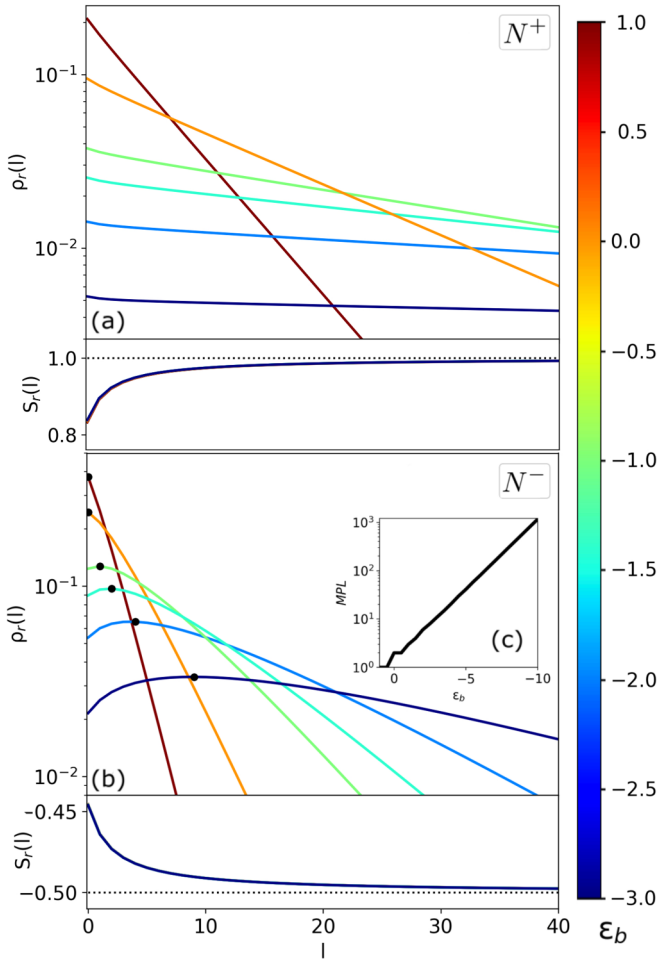
FIG. 2. Polymer molecular-weight distributions $\rho_{r\ell}$ and corresponding uniaxial nematic order parameter $S_{r\ell}$ as a function of the polymer length ℓ for (a) a typical polymer nematic N^+ and (b) discotic nematic phase N^-. The effective temperature ε_b is color-coded. (c) Most probable length (MPL) in terms of the effective temperature ε_b. Fixed parameters: persistence length $\ell_p = 3$, disk mole fraction $x = 0.5$, overall concentration $\rho = 3$, excluded-volume ratios $q = \frac{1}{4}\frac{L_r}{D_r}$ and $z = \pi q$ with monomer aspect ratio $L_r/D_r = 10$.

volumes. Our principal attention goes to the latter systems which arise more naturally in an experimental context when mixing, for instance, tip-associating colloidal rods such as *fd* [68,69] with clay platelets [70]. The molecular-weight distributions of some mixtures of this nature are shown in Fig. 2.

Figure 2(a) relates to the uniaxial polymer-dominated nematic phase (N^+) and demonstrates an exponential probability distribution whose shape can be tuned by changing the effective temperature of the system. As expected, the tail of the distribution grows longer upon decreasing the temperature, which would give longer polymers. A more interesting scenario shows up for the discotic nematic phase (N^-) in Fig. 2(b), where the distributions are no longer monotonically decreasing. The maximum of the distributions corresponds to the most probable length of the polymers for each system, which depends quite sensitively on the effective tempera-

ture as we observe in Fig. 2(c). Reversible polymerization within an antinematically organization thus leads to a strong manifestation of oligomeric polymers at the expense of its monomeric counterparts. We note that the orientational order associated with the antinematic oligomers remains relatively mild (particularly at larger temperature ε_b) so that the second-polynomial truncation should not be too severe.

As we will see in the following sections of this paper, the overall particle concentration and disk molar fraction associated with Fig. 2 may correspond to regions of the phase diagram where the uniform nematic system is in fact thermodynamically unstable with respect to some kind of phase separation. The molecular-weight distributions should therefore be interpreted under the caveat that monophasic nematic fluidity is preserved and that any demixing process is somehow suppressed. We wish to add that the nonmonotonic features of the antinematic polymer molecular-weight distribution are also present at conditions where monophasic antinematic order is found to be stable. Next we address the thermodynamic stability of the mixtures within the context of a Gaussian variational theory.

V. ISOTROPIC-NEMATIC PHASE BEHAVIOR

At conditions where (anti)nematic order is strong, the previously used polynomial-based expansion truncated after $\mathcal{P}_2$ [Eq. (7)] is no longer appropriate and a cumbersome inclusion of multiple higher-order terms becomes necessary [36,65]. A more technically expedient route towards exploring the thermodynamics of strongly ordered nematic fluids is to use a simple Gaussian parametrization of the orientational probability [17,18]. Following [61] we express the polymer molecular-weight distribution in a factorized form:

$$\rho_r(\ell, \hat{\mathbf{u}}) = \rho_{r\ell} f_G(\hat{\mathbf{u}}), \qquad (26)$$

where f_G is a normalized Gaussian distribution with a variational parameter that is proportional to either the amount of nematic order ($\alpha^{(1)} > 0$) or antinematic order ($\alpha^{(2)} > 0$). The corresponding Gaussian distributions for the polar angles corresponding to these different nematic symmetries are given by [35]:

$$f_G(\hat{\mathbf{u}}) \sim \begin{cases} \frac{\alpha^{(1)}}{4\pi} \exp\left(-\frac{1}{2}\alpha^{(1)}\theta^2\right), \\ \sqrt{\frac{\alpha^{(2)}}{(2\pi)^3}} \exp\left(-\frac{1}{2}\alpha^{(2)}\psi^2\right), \end{cases} \qquad (27)$$

where $\psi = \frac{\pi}{2} - \theta$ $(-\pi/2 < \psi < \pi/2)$ denotes a meridional angle [see Fig. 1(a)]. The Gaussians operates on the domain $0 < \theta < \pi/2$ and must be complemented by their mirror $f_G(\pi - \theta)$ for $\pi/2 < \theta < \pi$ given that all nematic phases are required to be strictly apolar. The Gaussian representations are appropriate only for strong nematic order ($\alpha \gg 1$). They are clearly inadequate for isotropic systems since the probabilities reduce to zero when $\alpha \to 0$ instead of reaching a constant. Obviously we apply the same distributions to the disks with $\alpha_d^{(1)}$ and $\alpha_d^{(2)}$ denoting the variational parameters

quantifying the amount of nematic or antinematic order, respectively. The disk probability density is then equivalent to Eq. (26):

$$\rho_d(\hat{\mathbf{u}}) = \rho_{d0} f_G(\hat{\mathbf{u}}). \qquad (28)$$

A major advantage of using Gaussian trial functions is that we may apply asymptotic expansion of the various free energy contributions [17] which are valid in the limit $\alpha \to \infty$. In particular, it can be shown that the double orientational averages over the sine and cosine in Eq. (4) up to leading order in α take a simple analytic form [35]. In the general case in which particles with equal nematic signature (nematic or antinematic) do not necessarily have the same degree of

alignment the asymptotic averages read:

$$\langle\langle |\sin\gamma|\rangle\rangle_{11} \sim \sqrt{\frac{\pi}{2}\left(\frac{1}{\alpha^{(1)}} + \frac{1}{\alpha^{(1\prime)}}\right)},$$

$$\langle\langle |\cos\gamma|\rangle\rangle_{12} \sim \sqrt{\frac{2}{\pi}\left(\frac{1}{\alpha^{(1)}} + \frac{1}{\alpha^{(2)}}\right)},$$

$$\langle\langle |\sin\gamma|\rangle\rangle_{22} \sim \mathcal{F}(\alpha^{(2)}, \alpha^{(2\prime)}). \qquad (29)$$

Here the double brackets denote the orientational averages featuring in the excess free energy (4) with $\langle\cdot\rangle = \int d\hat{\mathbf{u}} f_G(\hat{\mathbf{u}})$. The symmetry of nematic order clearly matters since the antinematic case features a distinct logarithmic dependence. The function $\mathcal{F}$ reads in explicit form:

$$\mathcal{F}(\alpha^{(2)}, \alpha^{(2\prime)}) = \frac{4\alpha^{(2)}Q - 2(1+Q)\mathrm{arctanh}\sqrt{Q} - (1+Q)\ln(1-Q) + (1+Q)\ln(4\alpha^{(2)}Q)}{2\pi\alpha^{(2)}Q} \qquad (30)$$

in terms of the ratio $Q = \alpha^{(2\prime)}/\alpha^{(2)}$ with $\alpha^{(2)}$ and $\alpha^{(2\prime)}$ quantifying the antinematic order parameters of two polymeric species differing in length. Note that generally, $\alpha^{(2)} \neq \alpha^{(2\prime)}$. The expression becomes a lot more manageable if all polymers are assumed to exhibit an equal degree of alignment, irrespective of their length. Then $Q = 1$ and [71]:

$$\mathcal{F}(\alpha^{(2)}) = \frac{2}{\pi}\left(1 + \frac{\ln\alpha^{(2)}}{2\alpha^{(2)}}\right). \qquad (31)$$

Similar asymptotic expressions may be obtained for the orientational entropy featuring in the ideal free energy Eq. (1). For strong nematic or antinematic order we find, respectively [35]:

$$\sigma_1 = \langle\ln 4\pi f_G(\hat{\mathbf{u}})\rangle_1 \sim \ln\alpha^{(1)} - 1,$$

$$\sigma_2 = \langle\ln 4\pi f_G(\hat{\mathbf{u}})\rangle_2 \sim \frac{1}{2}\left(\ln\alpha^{(2)} + \ln\frac{2}{\pi} - 1\right). \qquad (32)$$

The wormlike chain entropy (3) too can be quantified within the Gaussian limit which leads to:

$$\left\langle \ln f_G^{1/2}(\hat{\mathbf{u}})\nabla^2 f_G^{1/2}(\hat{\mathbf{u}})\right\rangle_1 \sim -\frac{\alpha^{(1)}}{2},$$

$$\left\langle \ln f_G^{1/2}(\hat{\mathbf{u}})\nabla^2 f_G^{1/2}(\hat{\mathbf{u}})\right\rangle_2 \sim -\frac{\alpha^{(2)}}{4}. \qquad (33)$$

We infer that the loss of conformational entropy of an *antinematic* polymer is half that of a nematic polymer. This suggests that a wormlike chain is able to retain more of its internal configurations when aligned antinematically than in a nematic organization of equal strength. With all the orientational averages specified, we now turn to computing the free energy and its derivatives.

A. Polymer nematic phase (N^+)

We first focus on the case of the polymer-dominated nematic phase which is expected to be stable at elevated monomer concentration and low disk mole fraction. Inserting the asymptotic orientational averages formulated above into

the corresponding entropic contributions in Eq. (1) we obtain the following algebraic expression for the free energy density (in units thermal energy $k_B T$ per randomized monomer excluded volume v_{rr}):

$$\begin{aligned}
\frac{F^{N^+}}{V} \sim &\sum_\ell \rho_{r\ell}\ell^{-1}[\ln\rho_{r\ell}\ell^{-1} - 1 - \varepsilon_b + \sigma_1(\alpha_{r\ell})] \\
&+ \rho_{d0}[\ln\rho_{d0} - 1 + \sigma_2(\alpha_d)] \\
&+ \frac{1}{3\ell_p}\sum_\ell \rho_{r\ell}\alpha_{r\ell} + \sum_{\ell,\ell'}\rho_{r\ell}\rho_{r\ell'}h_{r\ell r\ell'} \\
&+ 2q\rho_{d0}\sum_\ell \rho_{r\ell}h_{r\ell d} + z\rho_{d0}^2\frac{8}{\pi^2}\left(1 + \frac{\ln\alpha_d}{2\alpha_d}\right) \quad (34)
\end{aligned}$$

with h_{ij} is short-hand notation for:

$$h_{ij} = \sqrt{\frac{8}{\pi}\left(\frac{1}{\alpha_i} + \frac{1}{\alpha_j}\right)}, \qquad (35)$$

where α_i and α_j should be considered dummy variables for the species-dependent nematic order parameters as specified by the indices i and j. For later reference we also define:

$$g_{ij} = \left(\frac{8}{\pi}\right)^{1/2}\left(1 + \frac{\alpha_i}{\alpha_j}\right)^{-1/2}. \qquad (36)$$

At equilibrium, the species-dependent nematic order parameters $\alpha_{r\ell}$ and α_d follow from the minimum conditions:

$$\frac{\partial F/V}{\partial\alpha_{r\ell,d}} = 0. \qquad (37)$$

The expressions above can be simplified considerably by noting that a small amount of backbone flexibility causes the nematic alignment to fully decorrelate from the polymer contour length. We then approximate $\alpha_{r\ell} \approx \alpha_{r\ell'} = \alpha_r$, independent from ℓ. Applying Eq. (37) we obtain a set of simple

algebraic equations:

$$m_{N^+}^{-1}\alpha_r^{1/2} = -\frac{1}{3\ell_p}\alpha_r^{3/2} + \frac{2}{\sqrt{\pi}}\rho_{r0} + q\rho_{d0}g_{rd},$$

$$\alpha_d^{1/2} = z\rho_{d0}\frac{8}{\pi^2}\left(\frac{\ln\alpha_d - 1}{\alpha_d^{1/2}}\right) + 4q\rho_{r0}g_{dr}, \qquad (38)$$

with m_{N^+} the mean aggregation number in the polymer nematic phase. The molecular-weight distribution now becomes strictly exponential, as for the isotropic phase. We write:

$$\rho_{r\ell} = \ell e^{\tilde{\varepsilon}_b}\left(1 - m_{N^+}^{-1}\right)^{\ell} \qquad (39)$$

with an *effective* potential $\tilde{\varepsilon}_b$ that depends on the orientational entropy:

$$\tilde{\varepsilon}_b = \varepsilon_b - \sigma_1(\alpha_r). \qquad (40)$$

Given that $\sigma_1 > 0$, the effective temperature is *lower* than the bare one, so that polymerization in the nematic phase is stronger than in the isotropic fluid, as is well established [19,51]. The mean aggregation number in the nematic phase has an analogous form to Eq. (15):

$$m_{N^+} = \tfrac{1}{2}(1 + \sqrt{1 + 4\rho_{r0}e^{-\tilde{\varepsilon}_b}}). \qquad (41)$$

The chemical potentials are obtained from the standard thermodynamic relations $\mu_{r,d} = \partial(F/V)/\partial\rho_{r0,d0}$. The contribution from the polymers reads:

$$\mu_r^{N^+} \sim \ln\left(1 - m_{N^+}^{-1}\right) + \frac{1}{3\ell_p} + m_{N^+}^{-1}\sigma_1(\alpha_r)$$

$$+ 2\rho_{r0}\frac{4}{\sqrt{\pi\alpha_r}} + 2q\rho_{d0}h_{rd} + \varepsilon_b, \qquad (42)$$

while for the disks we find:

$$\mu_d^{N^+} \sim \ln\rho_{d0} + \sigma_2(\alpha_d) + 2q\rho_{r0}h_{rd} + 2z\rho_{d0}\frac{8}{\pi^2}\left(1 + \frac{\ln\alpha_d}{2\alpha_d}\right). \qquad (43)$$

The osmotic pressure follows from the thermodynamic relation $-P = (F - N\mu)/V$ leading to:

$$P^{N^+} \sim e^{\tilde{\varepsilon}_b}(m_{N^+} - 1) + \rho_{d0} + \rho_{r0}^2\frac{4}{\sqrt{\pi\alpha_r}}$$

$$+ 2q\rho_{r0}\rho_{d0}h_{rd} + z\rho_{d0}^2\frac{8}{\pi^2}\left(1 + \frac{\ln\alpha_d}{2\alpha_d}\right). \qquad (44)$$

Note that all pressures are implicitly renormalized in units of the thermal energy k_BT per monomer excluded volume v_{rr}.

B. Discotic nematic phase (N^-)

Repeating the previous steps for the discotic nematic through simple bookkeeping we write for the free energy of

the discotic phase:

$$\frac{F^{N^-}}{V} \sim \sum_{\ell}\rho_{r\ell}\ell^{-1}[\ln\rho_{r\ell}\ell^{-1} - 1 - \varepsilon_b + \sigma_2(\alpha_{r\ell})]$$

$$+ \rho_{d0}[\ln\rho_{d0} - 1 + \sigma_1(\alpha_d)] + \frac{1}{6\ell_p}\sum_{\ell}\rho_{r\ell}\alpha_{r\ell}$$

$$+ \sum_{\ell,\ell'}\rho_{r\ell}\rho_{r\ell'}\frac{4}{\pi}\mathcal{F}(\alpha_{r\ell}, \alpha_{r\ell'})$$

$$+ 2q\rho_{d0}\sum_{\ell}\rho_{r\ell}h_{r\ell d} + z\rho_{d0}^2\frac{4}{\sqrt{\pi\alpha_d}}. \qquad (45)$$

The corresponding minimum conditions for the variational parameters under the assumption that all polymer species experience the same degree of orientational order ($\alpha_{r\ell} = \alpha_{r\ell'} = \alpha_r$) are as follows:

$$\frac{1}{2}m_{N^-}^{-1}\alpha_r^{1/2} = -\frac{1}{6\ell_p}\alpha_r^{3/2} + \rho_{r0}\frac{8}{\pi^2}\left(\frac{\ln\alpha_r - 1}{\alpha_r^{1/2}}\right) + q\rho_{d0}g_{rd}$$

$$\alpha_d^{1/2} = z\rho_{d0}\frac{2}{\pi^{1/2}} + 2q\rho_{r0}g_{dr}. \qquad (46)$$

The molecular-weight distribution is analogous to Eq. (39) but with the effective temperature now reading:

$$\tilde{\varepsilon}_b = \varepsilon_b - \sigma_2(\alpha_r), \qquad (47)$$

which, as for the case of the polymer nematic phase suggests that particle alignment facilitates polymer growth, although less so for antinematic polymers since generally $\sigma_2 < \sigma_1$ [Eq. (32)]. The chemical potential of the polymers and the disks are given by, respectively:

$$\mu_r^{N^-} \sim \ln\left(1 - m_{N^-}^{-1}\right) + \frac{1}{6\ell_p} + m_{N^-}^{-1}\sigma_2(\alpha_r)$$

$$+ 2\rho_{r0}\frac{8}{\pi^2}\left(1 + \frac{\ln\alpha_r}{2\alpha_r}\right) + 2q\rho_{d0}h_{rd} + \varepsilon_b, \qquad (48)$$

$$\mu_d^{N^-} \sim \ln\rho_{d0} + \sigma_1(\alpha_d) + 2q\rho_{r0}h_{rd} + 2z\rho_{d0}\frac{4}{\sqrt{\pi\alpha_d}}.$$

Finally, the pressure of the N^- phase reads:

$$P^{N^-} \sim e^{\tilde{\varepsilon}_b}(m_{N^-} - 1) + \rho_{d0} + \rho_{r0}^2\frac{8}{\pi^2}\left(1 + \frac{\ln\alpha_r}{2\alpha_r}\right)$$

$$+ 2q\rho_{r0}\rho_{d0}h_{rd} + z\rho_{d0}^2\frac{4}{\sqrt{\pi\alpha_d}}. \qquad (49)$$

The thermodynamics of the isotropic phase is easily established from the original free energy (1) because the randomized excluded volumes becomes simple constants, namely, $\langle\langle|\sin\gamma|\rangle\rangle = \pi/4$ and $\langle\langle|\cos\gamma|\rangle\rangle = 1/2$. We thus obtain the following expressions for the chemical potentials in the isotropic fluid [61]:

$$\mu_r^{I} \sim \ln\left(1 - m_I^{-1}\right) + 2\rho_{r0} + 2q\rho_{d0} + \varepsilon_b,$$

$$\mu_d^{I} \sim \ln\rho_{d0} + 2z\rho_{d0} + 2q\rho_{r0}. \qquad (50)$$

The osmotic pressure combines the ideal gas and excluded volume contributions and reads:

$$P^{I} \sim e^{\varepsilon_b}(m_I - 1) + \rho_{d0} + \rho_{r0}^2 + 2q\rho_{r0}\rho_{d0} + z\rho_{d0}^2. \qquad (51)$$
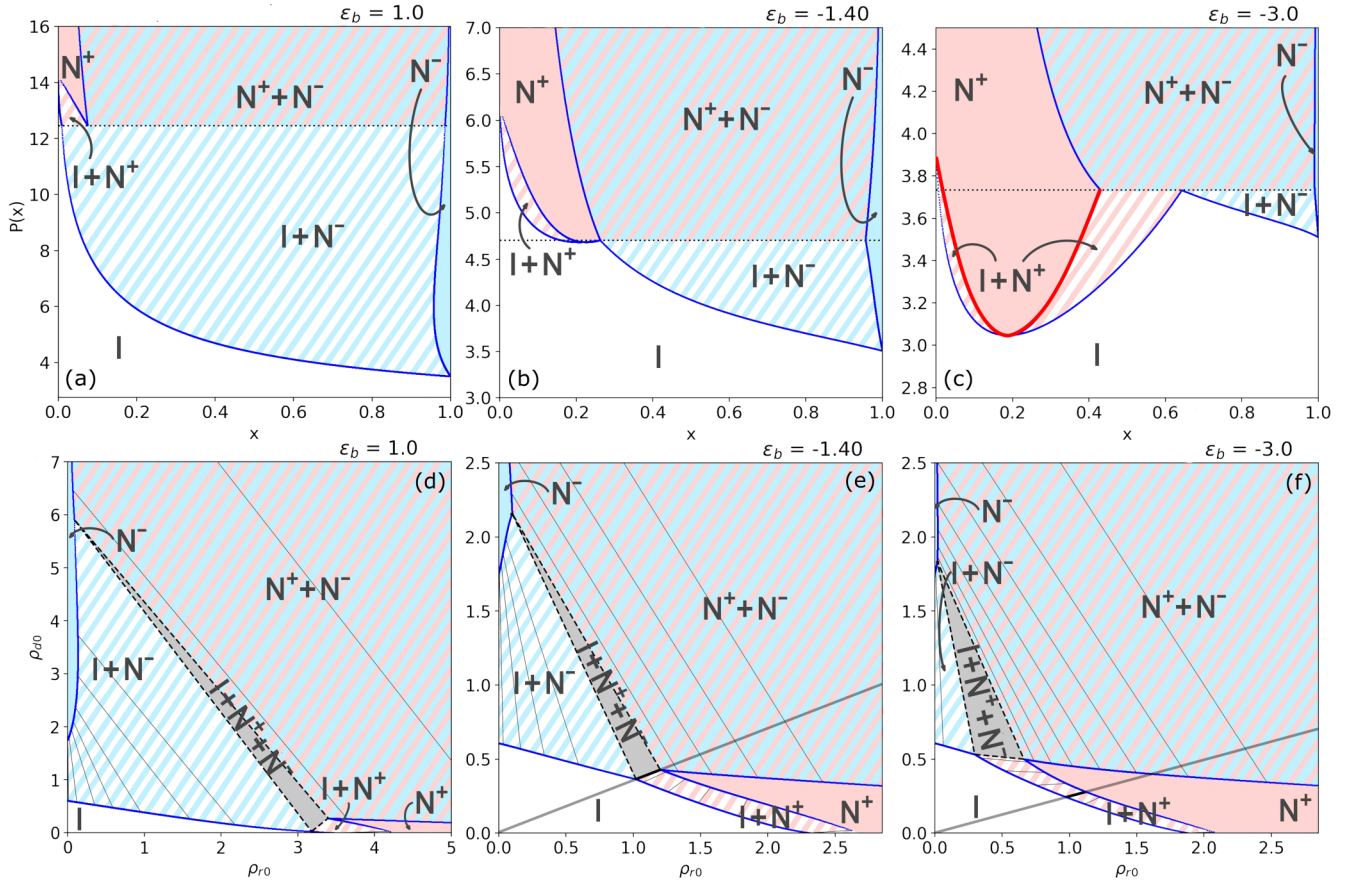
FIG. 3. Overview of the isotropic I (white), polymer nematic N^+ (red), and discotic nematic N^- (blue) phase diagrams for a mixture of disks and reversibly polymerizing weakly flexible rods at various effective temperatures ε_b. Two types of phase diagrams are represented: osmotic pressure P versus disk mole fraction x (top panels) and concentration of disks ρ_{d0} versus concentration of rods ρ_{r0} (bottom panels). Fixed parameters: persistence length $\ell_p = 3$, excluded-volume ratios $q = \frac{1}{4}\frac{L_r}{D_r}$ and $z = \pi q$ where $L_r/D_r = 10$. The presence of a negative azeotrope is indicated in panels (e) and (f) as a bold black line, which is shown to be parallel to the dilution line [gray diagonal shown in (e) and (f)].

Binodals denoting coexistence between phases of any symmetry may be established from equating chemical potentials and pressures in conjunction with the minimum conditions for the nematic variational parameters, where relevant. Phase diagrams can be represented in a pressure-composition ($P - x$) plane or, alternatively, in a density-density representation using $\rho_{r0} = c(1-x)$ and $\rho_{d0} = cx$ in terms of the overall particle concentration c and disk mole fraction ($0 < x < 1$). In order to remain consistent with the Gaussian approximation adopted in our analysis, we will focus on *asymmetric* mixtures characterized by both monomer-disk and disk-disk excluded volumes being much larger than the monomer-monomer one. The considerable excluded-volume disparity thus ensures that the nematic order of all components be sufficiently strong. Concretely, we impose that $\alpha_{r,d} > 5$ for all numerical results to be self-consistent.

VI. PHASE DIAGRAMS

Figure 3 presents an overview of the isotropic-nematic phase diagram for a mixture of reversibly polymerizing rods and disks at three different temperatures. The choice of excluded-volume parameter q and z is inspired by the typical

dimensions of experimentally realizable anisotropic colloids, where the monomeric rods and disks usually have *equal* largest dimensions ($L_r = D_d$). The monomer aspect ratio L_r/D_r can be chosen freely but we fix it here at $L_r/D_r = 10$. The disk aspect ratio is not constrained as long as the disks are sufficiently thin ($D_d/L_d \gg 1$). In this study we keep the persistence length fixed at $\ell_p = 3$. We found that variations up to $\ell_p = 10$ (corresponding to stiffer monomers) did not lead to major changes in the phase behavior. For practical reasons we refrained from exploring the near-rigid rod limit ($\ell_p \to \infty$) which is known to cause the polymers to grow to unphysically large lengths [19].

Several key trends in the phase diagrams can be discerned. First, Fig. 3(a) correspond to high-temperature scenario in which reversible polymerization happens on a very limited scale. The shape-dissimilar nature of the mixture translates into a phase diagram that is highly asymmetric about the equimolar point $x = 0.5$. Second, demixing is prominent given the large range of monomer-disk compositions where the mixture fractionates into strongly segregated uniaxial nematic phases [Fig. 3(a)]. Only at very low osmotic pressures, where particle exclusion effects are relatively weak, does the mixture remain miscible throughout the entire composition
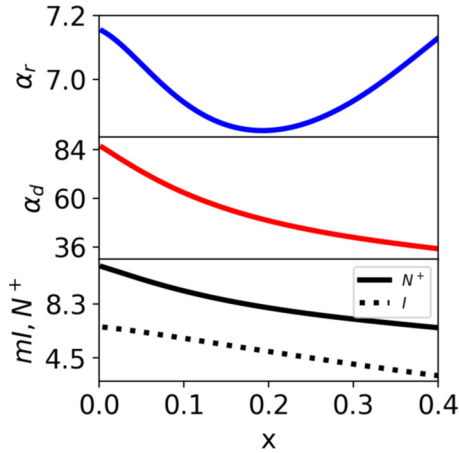
FIG. 4. Nematic order of the polymers (α_r) and disks (α_d) and polymer mean aggregation number (m) of the nematic N^+ phase in coexistence with the isotropic phase I across the azeotropic region. The corresponding binodal in Fig. 3(c) has been indicated in red.

range. We further observe that the discotic nematic N^- can be stabilized over a relatively broad pressure range, while the polymer nematic (N^+) only features at elevated pressures, where polymerization is strong enough for the long polymers to align into a conventional nematic organization with the disks interspersed antinematically. The phase diagram also features a triple $I - N^+ - N^-$ equilibrium in agreement with previous predictions [34,35] and experiment [57,59] for disks mixed with *non*polymerizing rods.

Reducing the temperature stimulates polymer growth and, consequently, enhances the stability window for the polymer-dominated nematic [Figs. 3(b) and 3(c)]. Reversible polymerization thus renders the phase diagrams less asymmetric. At the same time, the osmotic pressure (and concomitantly the particle concentrations) at which nematic order occurs drops significantly as polymerization becomes more prominent. Furthermore, the $I - N^+$ binodals develop a remarkable (negative) *azeotrope* which in Fig. 3(b) coincides with the triple pressure. Under these conditions, coexistence occurs between a discotic nematic, a polymer nematic and an isotropic fluid with the latter two having the same monomer-disk composition. At lower temperature the azeotrope comes out more prominently at $x \approx 0.2$ [Fig. 3(c)]. In the density-density representations shown in the bottom panels, the azeotrope manifests itself at the point where the tie line connecting the monomer and disks concentrations of the coexisting I and N^+ phases coincides with the dilution line. The latter are straight lines emanating from the origin along which the overall particle concentration changes but the monomer-disk composition is preserved. It can be gleaned that upon following a dilution line at, for instance, $x = 0.2$ the sequence of phase transitions encountered depends strongly on temperature. At high temperature [Fig. 3(a)] the isotropic fluid first transforms into N^-, then develops a triphasic $I - N^+ - N^-$ equilibrium. At low temperature, however, a polymer nematic is formed first, followed by a binematic $N^+ - N^-$ coexistence while the triphasic equilibrium does not show up at all unless the monomer concentration is significantly increased. Figure 4 provides insight into the change of nematic order of the

polymers and disks as well as the mean aggregation number of the N^+ across the azeotrope. In view of their considerable excluded volume, the disks are way more ordered than the polymers ($\alpha_d > \alpha_r$). Increasing the mole fraction of disks reduces the nematic order of both components, though the decrease is much more significant for the disks than the change of α_r for the polymers which in fact develops a minimum at the azeotrope.

We move on to explore a similar mixture featuring more slender rod monomers, namely, $L_r/D_r = 25$. The resulting phase diagram is shown in Fig. 5. The asymmetry of the mixture is now very strong with the monophasic N^+ and N^- regions being largely unstable except for strongly purified systems (x close to 0 or 1) [Fig. 5(b)]. Qualitatively, the phase diagram resembles the one in Fig. 3(a), but the isotropic fluid undergoes a gas-liquid-type phase separation producing two phases differing in composition. The I_1-phase may be associated with a discotic colloidal gas, and I_2 with its liquid counterpart. The demixing is driven by the extreme excluded-volume difference between the rod monomers and the disks. This phenomenon has been reported for (nonpolymerizing) rod-disk mixtures in Ref. [33], where the effect was ascribed to a *depletion* of disks by the much smaller rods. Isotropic-isotropic demixing has been more generally observed when mixing different shapes dominated by hardcore repulsion [72], including thin and thick rods [73], spheres and disks [74,75], and disks differing in diameter [76]. It has also been observed in thermotropic LC-solvent mixtures where the effect is primarily of enthalpic origin and is caused by specific interactions between the LC forming molecules and the solvent [77,78]. It is well known that mixing colloids with nonadsorbing polymer depletants creates an effective attraction between the colloids which is entirely of entropic origin and may drive various types of demixing mechanisms [79]. In our case, the depletion effect is however less clearcut given that the "depletants" reversibly polymerize into a wide array of different sizes [80] and experience orientation-dependent volume-exclusion interactions, which are usually ignored in colloid-polymer models. Moreover the average polymer size depends, via Eq. (15), on the monomer concentration which is different in the gas and liquid phases. Figure 5(c) demonstrates that the difference in mean aggregation number between the two isotropic phases is in fact quite small, with the disk-rich fraction harboring slightly longer polymers. Note that the presence of isotropic-isotropic demixing gives rise to a low-pressure triple equilibrium where both phases coexist with a discotic nematic N^-.

VII. QUADRUPLE FLUID COEXISTENCE

At this stage, one might wonder whether a mixtures could be designed in which the two separate triple equilibria in Fig. 5 were to join into a *quadruple* coexistence featuring all fluid phases. In Fig. 6(a) we demonstrate that this scenario is indeed possible. For the particular mixture shown there, the rod monomers and disks no longer have equal largest dimensions ($L_r = D_d$) but the disk diameter is somewhat smaller than the rod length, namely $D_d = 0.7L_r$ while the rods are kept sufficiently slender ($L_r/D_r = 25$). The excluded-volume asymmetry is then sufficiently reduced to make the two triple
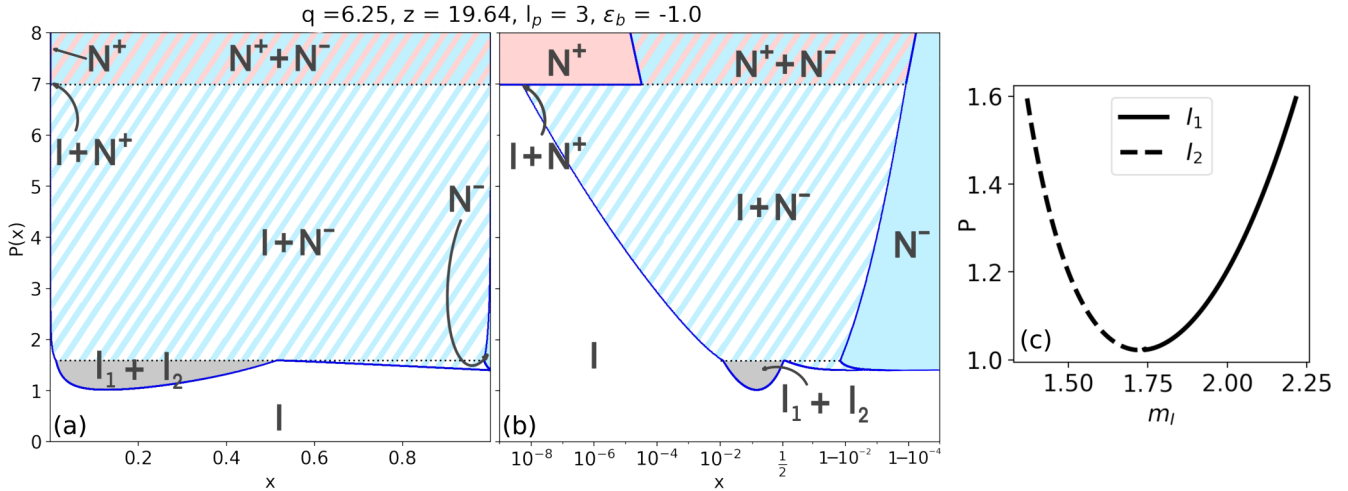
FIG. 5. Phase diagram in the osmotic pressure-composition $(P - x)$ representation with the following parameters: persistence length $\ell_p = 3$, effective temperature $\varepsilon_b = -1$, excluded-volume *ratios* $q = \frac{1}{4}\frac{L_r}{D_r}$, and $z = \pi q$ corresponding to a monomer aspect ratio $L_r/D_r = 25$. The disk mole fraction x is plotted on a linear scale (a) and on a logarithmic scale (b) to highlight the behavior close to single-component systems (pure polymers $x = 0$, and pure disks $x = 1$). Note the presence of a coexistence between an isotropic gas and fluid phase (I_1 and I_2) with different disks compositions (gray region). (c) Comparison of mean aggregation numbers m_I between I_1 and I_2 for a given pressure. I_1 corresponds to the phase with the lowest disk mole fraction x.

points coincide and generate a simultaneous coexistence between two isotropic and two nematic phases, each differing in monomer-disk composition and overall particle concentration. This mixture is by no means unique and belongs to a family of monomer-disk size ratios where a remarkable I_1-I_2-N^+-N^- quadruple point could be encountered, as illustrated by the colored manifold in Fig. 6(b). This result provides important guidance if one wishes to explore these intricate multiphase equilibria in real-life mixtures featuring reversibly polymerizing rods mixed with colloidal platelets.

At this point we wish to draw a connection with recent theoretical explorations of polymer depletion on purely monomeric colloidal rods which have revealed similar multiphase equilibria involving one-dimensional periodic smectic structures as well as fully crystalline states [81]. Similar

FIG. 6. (a) Phase diagram in the osmotic pressure-composition $(P - x)$ representation showing an I_1-I_2-N^+-N^- quadruple point at $P = 4.29$. For this particular case, $\ell_p = 3$, $\varepsilon_b = -1.2$, $L_r/D_r = 25$ and $D_d/L_r = 0.7$. (b) Visualization of combinations of rod-disk excluded-volume ratio (q and z) and temperature ε_b where an $I_1 - I_2 - N^+ - N^-$ quadruple coexistence is possible.

phenomena involving isotropic-nematic-columnar quadruple points had been reported previously for disk-polymer mixtures [82]. In those studies, the multiphase equilibria emerge from an effective one-component theory based on free-volume theory where polymeric depletants, envisaged as fixed-shape spherical particles that do not interact with one another, are depleted from the surface of the colloidal rod due to volume exclusion as per the original Asakura-Oosawa model [83–85]. In our work, the depletion effect is strongly convoluted since all components (polymer species and disks alike) are explicitly correlated, albeit on the simplified second-virial level. Furthermore, high-density crystal phases with long-ranged positional order are not considered in the present study since their stability requires strong uniformity in particle shape [86], which is not the case in our mixtures. In fact, even for basic mixtures of nonassociating hard rods mixed with hard disks the full phase behavior at conditions of elevated particle packing remains largely elusive to this day. Large-scale numerical simulations or density-functional computations are needed to overcome the limitations of the simple second-virial approach taken here, but these are technically challenging to implement for dense multicomponent systems.

The results gathered in Fig. 6 illustrates the possibility of generating four different fluid textures emerging from reversibly changing excluded-volume-driven interactions alone, without the need to invoke attractive interparticle forces. This could bear some relevance on the emergence of functionality through liquid-liquid type phase separation in biological cells which are composed of biomolecules possessing a multitude of different shapes, some of them controlled by reversible association [87,88].
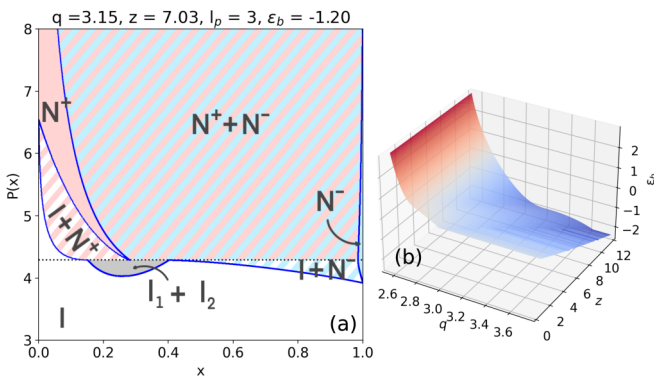
VIII. CONCLUSIONS

We have explored the phase behavior of a simple model for thermoresponsive supramolecular rods mixed with discotic

particles. Possessing attractive tips the rod monomers reversibly associate into polymers that retain their basic slender rod shape and experience only a limited degree of backbone flexibility. The interaction between the species is assumed to be of steric origin such that basic shape differences between the constituents, more specifically the excluded-volume disparity, plays a key role in determining the prevailing liquid crystal symmetry. The principal ones are a polymer nematic (N^+) composed of nematic polymer interspersed with an antinematic organization of disks and a discotic nematic (N^-) in which the polymers are dispersed antinematically. Lowering temperature stimulates polymer growth which enlarges the stability window for the N^+ phase. The phase diagram develops a marked *azeotrope* upon increasing the mole fraction of added disks which indicated that the polymer nematic is stabilized by the addition of nonadsorbing rigid disks provided their mole fraction remains small. The polymer-dominated nematic phase eventually becomes destabilized at larger mole fractions where mutual disk alignment disrupts the nematic order of the polymers in favor of the formation of a discotic nematic phase in which the polymers self-organize into an antinematic structure. The corresponding molecular weight distribution functions strongly deviates from the usual exponential form and becomes nonmonotonic with a maximum probability associated with oligomeric aggregates. Enhancing the shape asymmetry between the rod monomers and disks we observe a depletion-driven demixing of the isotropic fluid which opens up the possibility of a quadruple existence featuring two isotropic phase along with the fractionated polymer and discotic nematic phases. Such quadruple points occur in a wide range of mixed-shape nematics involving supramolecular rods templated by disks and highlight the possibility of multiple liquid symmetries (both isotropic and anisotropic) coexisting in mixtures of anisotropic colloids with reversible and thermoresponsive shape-asymmetry without cohesive interparticle forces. Future explorations should aim at a more careful assessment of biaxial nematic order, ignored in the present study, which could develop in near-equimolar rod-disk mixtures provided they are stable against global demixing. Polymerizing rods and disks with finite particle thickness and low shape asymmetry may favor the emergence of liquid crystals possessing lamellar, columnar or fully crystalline signatures [89] which may be addressed using computer simulation models along the lines of Refs. [21,22,42]. Inspiration for such mixed-shape lamellar structures could be drawn from bio-inspired supramolecular liquid crystals [90] such as, for example, the "sliding columnar phase" and similar stacked architectures observed in cationic lyposome-DNA complexes [91,92] which are essentially made up of mixed planar and rod-shaped architectures.

The data that support the findings of this study are available from the corresponding author upon reasonable request.

APPENDIX: RENORMALIZED $\mathcal{P}_2$ APPROXIMATION FOR SLIGHTLY FLEXIBLE POLYMERS

We seek a simple perturbation theory for the one-body density Eq. (11) of near-rigid polymers characterized by a finite persistence length ℓ_p. Let us attempt the following generalization of the probability density distribution for the polymers:

$$\rho_r(\ell, \hat{\mathbf{u}}) = \ell e^{\varepsilon_b + \lambda_r \ell} e^{\ell(a_r + \xi)\mathcal{P}_2(\hat{\mathbf{u}})} \tag{A1}$$

with ξ representing a correction induced by the *internal* orientational entropy of the polymer due to a small degree of wormlike chain flexibility. Inserting this expression into the wormlike chain contribution (last term) in the EL equation (11), substituting $\nabla^2 = \partial_t(1 - t^2)\partial_t$ and $t = \cos\theta$, we find that for the uniaxial symmetry:

$$\frac{\nabla^2 \rho_r^{1/2}}{\rho_r^{1/2}} = \frac{3}{4}\tilde{a}_r^2 + \left(\frac{3}{2}\tilde{a}_r^2 - 3\tilde{a}_r\right)\mathcal{P}_2(t) + \mathcal{O}(t^4), \tag{A2}$$

where $\tilde{a}_r = a_r + \xi$ denotes a rescaled alignment amplitude for the polymer.

1. Antinematic polymers

We expect that neglecting the fourth-order term will be fairly harmless in a strongly antinematic state where t is generally very small (since $\theta \sim \pi/2$ for most polymers). This situation is naturally encountered in the N^- phase where $a_r \ell \ll 0$ in particular for long polymers. The constant in Eq. (A2) is unimportant for the EL equation where it can be subsumed into the normalization factor λ, but must be retained when computing the wormlike chain free energy. Then, consistency requires that:

$$\xi \approx \frac{1}{3\ell_p}\left(\frac{3}{2}\tilde{a}_r^2 - 3\tilde{a}_r\right), \tag{A3}$$

where the chain persistence length ℓ_p should be interpreted in units of the segment length L_r. From the above the dependence of ξ on the bare alignment amplitude a_r is easily resolved and we find:

$$\xi \approx 1 + \ell_p + |a_r| - \sqrt{(1 + \ell_p)^2 + 2|a_r|\ell_p}, \quad (a_r \ll 0). \tag{A4}$$

The correction factor vanishes in the rigid rod limit, $\lim_{\ell_p \to \infty} \xi = 0$, as it should.

2. Nematic polymers

We may repeat the analysis for the case of conventional nematic polymers as encountered in the polymer-dominated N^+ phase using a slightly different route. For $a_r \gg 1$ the average polar deflection angle will be small and we may expand the wormlike chain term up to quadratic order in θ. Using the asymptotic relation $\mathcal{P}_2(t) \sim 1 - 3\theta^2/2$ and ignoring any constant factors we find a simple approximation valid for $|t|$ close to unity (strong alignment):

$$\frac{\nabla^2 \rho_r^{1/2}}{\rho_r^{1/2}} \sim -\frac{3}{2}\left(\tilde{a}_r^2 + 2\tilde{a}_r\right)\mathcal{P}_2(t). \tag{A5}$$

Then, in analogy with the preceding case, we find an expression identical to Eq. (A4) except for a minus sign:

$$-\xi \approx 1 + \ell_p + |a_r| - \sqrt{(1 + \ell_p)^2 + 2|a_r|\ell_p}, \quad (a_r \gg 0).$$
(A6)

This simple scaling result confirms our expectation, namely that a small degree of backbone flexibility leads to a reduction of the alignment propensity for the polymers, since $|a_r + \xi|$ is always smaller than $|a_r|$. For strongly aligned systems, this effect turns out to be of equal strength for both nematic and antinematically ordered polymers.

[1] M. E. Cates, Macromolecules **20**, 2289 (1987).

[2] M. E. Cates, J. Phys. France **49**, 1593 (1988).

[3] G. Riess, Prog. Polym. Sci. **28**, 1107 (2003).

[4] A. Blanazs, S. P. Armes, and A. J. Ryan, Macromol. Rapid Commun. **30**, 267 (2009).

[5] C. De Michele, L. Rovigatti, T. Bellini, and F. Sciortino, Soft Matter **8**, 8388 (2012).

[6] C. De Michele, G. Zanchetta, T. Bellini, E. Frezza, and A. Ferrarini, ACS Macro Lett. **5**, 208 (2016).

[7] J. Lydon, J. Mater. Chem. **20**, 10071 (2010).

[8] S.-W. Tam-Chang and L. Huang, Chem. Commun. **17**, 1957 (2008).

[9] T. P. J. Knowles and M. J. Buehler, Nat. Nanotechnol. **6**, 469 (2011).

[10] E. Fuchs and D. W. Cleveland, Science **279**, 514 (1998).

[11] F. Gittes, B. Mickey, J. Nettleton, and J. Howard, J. Cell Biol. **120**, 923 (1993).

[12] J. F. Berret, D. C. Roux, G. Porte, and P. Lindner, Europhys. Lett. **25**, 521 (1994).

[13] M. Nakata, G. Zanchetta, B. D. Chapman, C. D. Jones, J. O. Cross, R. Pindak, T. Bellini, and N. A. Clark, Science **318**, 1276 (2007).

[14] P. G. de Gennes and J. Prost, *The Physics of Liquid Crystals* (Clarendon Press, Oxford, 1993).

[15] A. Matsuyama and T. Kato, J. Phys. Soc. Jpn. **67**, 204 (1998).

[16] L. Onsager, Ann. N. Y. Acad. Sci. **51**, 627 (1949).

[17] T. Odijk, Macromolecules **19**, 2313 (1986).

[18] G. J. Vroege and H. N. W. Lekkerkerker, Rep. Prog. Phys. **55**, 1241 (1992).

[19] P. van der Schoot and M. E. Cates, Langmuir **10**, 670 (1994).

[20] J. T. Kindt and W. M. Gelbart, J. Chem. Phys. **114**, 1432 (2001).

[21] T. Kuriabova, M. D. Betterton, and M. A. Glaser, J. Mater. Chem. **20**, 10366 (2010).

[22] K. T. Nguyen, F. Sciortino, and C. De Michele, Langmuir **30**, 4814 (2014).

[23] L. Tortora, H.-S. Park, S.-W. Kang, V. Savaryn, S.-H. Hong, K. Kaznatcheev, D. Finotello, S. Sprunt, S. Kumar, and O. D. Lavrentovich, Soft Matter **6**, 4157 (2010).

[24] R. Kato, A. Kakugo, K. Shikinaka, Y. Ohsedo, A. M. R. Kabir, and N. Miyamoto, ACS Omega **3**, 14869 (2018).

[25] R. Alben, J. Chem. Phys. **59**, 4299 (1973).

[26] A. Stroobants and H. N. W. Lekkerkerker, J. Phys. Chem. **88**, 3669 (1984).

[27] P. J. Camp, M. P. Allen, P. G. Bolhuis, and D. Frenkel, J. Chem. Phys. **106**, 9270 (1997).

[28] E. Sokolova and A. Vlasov, J. Phys. Condes. Matter **9**, 4089 (1997).

[29] A. G. Vanakaras, S. C. McGrother, G. Jackson, and D. J. Photinos, Mol. Cryst. Liq. Cryst. **323**, 199 (1998).

[30] A. G. Vanakaras, A. F. Terzis, and D. J. Photinos, Mol. Cryst. Liq. Cryst. **362**, 67 (2001).

[31] H. Matsuda, T. Koda, S. Ikeda, and H. Kimura, J. Phys. Soc. Jpn. **72**, 2243 (2003).

[32] S. Varga, A. Galindo, and G. Jackson, J. Chem. Phys. **117**, 10412 (2002).

[33] S. Varga, A. Galindo, and G. Jackson, J. Chem. Phys. **117**, 7207 (2002).

[34] A. Galindo, A. J. Haslam, S. Varga, G. Jackson, A. G. Vanakaras, D. J. Photinos, and D. A. Dunmur, J. Chem. Phys. **119**, 5216 (2003).

[35] H. H. Wensink, G. J. Vroege, and H. N. W. Lekkerkerker, J. Chem. Phys. **115**, 7319 (2001).

[36] H. H. Wensink, G. J. Vroege, and H. N. W. Lekkerkerker, Phys. Rev. E **66**, 041704 (2002).

[37] A. Matsuyama, J. Chem. Phys. **132**, 214902 (2010).

[38] H. Mundoor, S. Park, B. Senyuk, H. H. Wensink, and I. I. Smalyukh, Science **360**, 768 (2018).

[39] C. Avendaño, G. Jackson, E. A. Müller, and F. A. Escobedo, Proc. Natl. Acad. Sci. USA **113**, 9699 (2016).

[40] H. H. Wensink and C. Avendaño, Phys. Rev. E **94**, 062704 (2016).

[41] I. Dozov, E. Paineau, P. Davidson, K. Antonova, C. Baravian, I. Bihannic, and L. J. Michot, J. Phys. Chem. B **115**, 7751 (2011).

[42] S. D. Peroukidis, S. H. L. Klapp, and A. G. Vanakaras, Soft Matter **16**, 10667 (2020).

[43] Y. Lyatskaya and A. C. Balazs, Macromolecules **31**, 6676 (1998).

[44] V. V. Ginzburg, C. Singh, and A. C. Balazs, Macromolecules **33**, 1089 (2000).

[45] F. M. van der Kooij and H. N. W. Lekkerkerker, J. Phys. Chem. B **102**, 7829 (1998).

[46] J. C. P. Gabriel, C. Sanchez, and P. Davidson, J. Phys. Chem. **100**, 11139 (1996).

[47] L. J. Michot, I. Bihannic, S. Maddi, S. S. Funari, C. Baravian, P. Levitz, and P. Davidson, Proc. Natl. Acad. Sci. USA **103**, 16101 (2006).

[48] E. Paineau, K. Antonova, C. Baravian, I. Bihannic, P. Davidson, I. Dozov, M. Imperor-Clerc, P. Levitz, A. Madsen, F. Meneau, and L. J. Michot, J. Phys. Chem. B **113**, 15858 (2009).

[49] P. van der Asdonk and P. H. J. Kouwer, Chem. Soc. Rev. **46**, 5935 (2017).

[50] M. P. Taylor and J. Herzfeld, Phys. Rev. A **43**, 1892 (1991).

[51] P. van der Schoot and M. E. Cates, Europhys. Lett. **25**, 515 (1994).

[52] S. Varga, A. Galindo, and G. Jackson, Phys. Rev. E **66**, 011707 (2002).

[53] P. van der Schoot, J. Chem. Phys. **104**, 1130 (1996).

[54] D. Frenkel, Liq. Cryst. **5**, 929 (1989).

[55] J. A. C. Veerman and D. Frenkel, Phys. Rev. A **45**, 5632 (1992).

[56] F. M. van der Kooij, K. Kassapidou, and H. N. W. Lekkerkerker, Nature (London) **406**, 868 (2000).

[57] F. M. van der Kooij and H. N. W. Lekkerkerker, Langmuir **16**, 10144 (2000).

[58] F. M. van der Kooij and H. N. W. Lekkerkerker, Phys. Rev. Lett. **84**, 781 (2000).

[59] P. Woolston and J. S. van Duijneveldt, Langmuir **31**, 9290 (2015).

[60] A. Galindo, G. Jackson, and D. J. Photinos, Chem. Phys. Lett. **325**, 631 (2000).

[61] H. H. Wensink, Macromolecules **52**, 7994 (2019).

[62] A. R. Khokhlov and A. N. Semenov, Phys. A **112**, 605 (1982).

[63] K. Lakatos, J. Stat. Phys. **2**, 121 (1970).

[64] R. F. Kayser and H. J. Raveche, Phys. Rev. A **17**, 2067 (1978).

[65] H. N. W. Lekkerkerker, P. Coulon, R. van der Hagen, and R. Deblieck, J. Chem. Phys. **80**, 3427 (1984).

[66] A. Speranza and P. Sollich, J. Chem. Phys. **117**, 5421 (2002).

[67] M. Abramowitz and I. A. Stegun, *Handbook of Mathematical Functions* (Dover, New York, 1973).

[68] S. Fraden, in *Observation, Prediction and Simulation of Phase Transitions in Complex Fluids*, edited by M. Baus (Springer, Dordrecht, 1995).

[69] Z. Dogic and S. Fraden, Curr. Opin. Colloid Interface Sci. **11**, 47 (2006).

[70] P. Davidson and J. C. P. Gabriel, Curr. Opin. Colloid Interface Sci. **9**, 377 (2005).

[71] H. H. Wensink, G. J. Vroege, and H. N. W. Lekkerkerker, J. Phys. Chem. B **105**, 10610 (2001).

[72] M. Dijkstra, D. Frenkel, and J.-P. Hansen, J. Chem. Phys. **101**, 3179 (1994).

[73] M. Dijkstra and R. van Roij, Phys. Rev. E **56**, 5594 (1997).

[74] M. Chen, H. Li, Y. Chen, A. F. Mejia, X. Wang, and Z. Cheng, Soft Matter **11**, 5775 (2015).

[75] R. Aliabadi, M. Moradi, and S. Varga, J. Chem. Phys. **144**, 074902 (2016).

[76] J. Phillips and M. Schmidt, Phys. Rev. E **81**, 041401 (2010).

[77] A. Matsuyama and T. Kato, J. Chem. Phys. **105**, 1654 (1996).

[78] C. G. Reyes, J. Baller, T. Araki, and J. P. F. Lagerwall, Soft Matter **15**, 6044 (2019).

[79] H. N. W. Lekkerkerker and R. Tuinier, *Colloids and the Depletion Interaction*, Lecture Notes in Physics, Vol. 833 (Springer, Dordrecht, 2011).

[80] V. F. D. Peters, M. Vis, and R. Tuinier, J. Polym. Sci. **59**, 1175 (2021).

[81] V. F. D. Peters, M. Vis, A. G. García, H. H. Wensink, and R. Tuinier, Phys. Rev. Lett. **125**, 127803 (2020).

[82] A. González García, H. H. Wensink, H. N. W. Lekkerkerker, and R. Tuinier, Sci. Rep. **7**, 17058 (2017).

[83] S. Asakura and F. Oosawa, J. Chem. Phys. **22**, 1255 (1954).

[84] S. Asakura and F. Oosawa, J. Pol. Sci. **33**, 183 (1958).

[85] A. Vrij, Pure Appl. Chem. **48**, 471 (1976).

[86] L. Mederos, E. Velasco, and Y. Martinez-Raton, J. Phys. Condens. Matter **26**, 463101 (2014).

[87] A. A. Hyman, A. C. Weber, and F. Jülicher, Annu. Rev. Cell Dev. Biol. **30**, 39 (2014).

[88] Y. Shin and C. P. Brangwynne, Science **357**, eaaf4382 (2017).

[89] S. D. Peroukidis, A. G. Vanakaras, and D. J. Photinos, J. Mater. Chem. **20**, 10495 (2010).

[90] C. R. Safinya, J. Deek, R. Beck, J. B. Jones, C. Leal, K. K. Ewert, and Y. Li, Liq. Cryst. **40**, 1748 (2013).

[91] G. C. L. Wong, J. X. Tang, A. Lin, Y. L. Li, P. A. Janmey, and C. R. Safinya, Science **288**, 2035 (2000).

[92] C. S. O'Hern and T. C. Lubensky, Phys. Rev. Lett. **80**, 4345 (1998).